Sea Surface Salinity And Barrier Layer Variability In The Equatorial Pacific As Seen From Aquarius And Argo

T. D. Qu, Y. T. Song, C. Maes

JOURNAL OF GEOPHYSICAL RESEARCH: OCEANS, VOL. 119, 15–29, doi:10.1002/2013JC009375, 2014

Sea surface salinity and barrier layer variability in the equatorial Pacific as seen from Aquarius and Argo

Tangdong Qu,[1] Y. Tony Song,[2] and Christophe Maes[3]

Received 23 August 2013; revised 20 November 2013; accepted 9 December 2013; published 7 January 2014.

[1] This study investigates the sea surface salinity (SSS) and barrier layer variability in the equatorial Pacific using recently available Aquarius and Argo data. Comparison between the two data sets indicates that Aquarius is able to capture most of the SSS features identified by Argo. Despite some discrepancies in the mean value, the SSS from the two data sets shows essentially the same seasonal cycle in both magnitude and phase. For the period of observation between August 2011 and July 2013 Aquarius nicely resolved the zonal displacement of the SSS front along the equator, showing its observing capacity of the western Pacific warm pool. Analysis of the Argo data provides further information on surface stratification. A thick barrier layer is present on the western side of the SSS front during all the period of observation, moving back and forth along the equator with its correlation with the Southern Oscillation Index exceeding 0.80. Generally, the thick barrier layer moves eastward during El Niño and westward during La Niña. The mechanisms responsible for this zonal displacement are discussed.

Citation: Qu, T., Y. T. Song, and C. Maes (2014), Sea surface salinity and barrier layer variability in the equatorial Pacific as seen from Aquarius and Argo, *J. Geophys. Res. Oceans*, *119*, 15–29, doi:10.1002/2013JC009375.

1. Introduction

[2] As the warmest open-ocean water in the global ocean, the western Pacific warm pool plays an important role in the world's climate [e.g., *Lukas et al*., 1996]. This warm water pool, characterized by sea surface temperature (SST) warmer than 28°C–29°C, lies between about 10°N and 15°S west of 160°W (Figure 1a), covering a global surface area equivalent to about two thirds of the continental United States. Although SST variability within the western Pacific warm pool is relatively small, its impact on the global atmosphere is large [e.g., *Palmer and Mansfield*, 1984], because of the vigorous atmospheric deep convection there. The western Pacific warm pool has been shown to migrate zonally on an interannual time scale ranging from 2 to 7 years, in response to the atmospheric and oceanic fluctuations associated with El Niño-Southern Oscillation (ENSO) [e.g., *McPhaden and Picaut*, 1990].

[3] The western Pacific warm pool is also a fresh water pool, and its eastern edge is characterized by a zonal sea surface salinity (SSS) front, which has a mean equatorial position near the international dateline (Figure 1b). The zonal SSS front separates the fresh western Pacific water from relatively salty central Pacific water, and the associated SSS gradient can reach as large as 1 psu (the values according to the 1978 practical salinity scale are given in psu for simplification in the rest of the text) in 1° longitude [*Rodier et al*., 2000; *Delcroix and McPhaden*, 2002; *Maes*, 2008]. Such a large SSS gradient is believed to play a role in the warm pool heat balance [e.g., *Shinoda and Lukas*, 1995; *Chen*, 2004]. According to previous studies, this SSS front can move eastward by up to 8000 km during an El Niño event [e.g., *Maes et al*., 2004], consistent with the revised theory for the oscillatory nature of ENSO by focusing on the advective feedback alone [*Picaut et al*., 1997].

[4] Another important feature of the western Pacific warm pool is the presence of the barrier layer. Due to a large excess of precipitation over evaporation (P-E), salinity in the upper western equatorial Pacific is low (<34.5 psu), compared with that in the central equatorial Pacific (>35.0 psu; Figure 1). The importance of this SSS contrast in surface stratification was first noted by *Godfrey and Lindstrom* [1989] and *Lukas and Lindstrom* [1991]. Their hydrographic observations revealed a unique vertical profile of temperature and salinity: a shallow fresh surface lens is embedded at the top of a deep isothermal layer. The shallow halocline marks the depth of the surface mixed layer, and the layer between the bottom of the mixed layer and the top of the thermocline was termed the "barrier layer" [*Lukas and Lindstrom*, 1991].

[5] The barrier layer is believed to play a role in the maintenance and temporal evolution of the western Pacific warm pool. Results from a coupled ocean-atmosphere general circulation model have clearly demonstrated that by isolating the mixed layer from the entrainment cooling at depth and by confining the response of westerly wind

[1]International Pacific Research Center, SOEST, University of Hawaii at Manoa, Honolulu, Hawaii, USA.
[2]Jet Propulsion Laboratory, California Institute of Technology, Pasadena, California, USA.
[3]Institut de Recherche pour le Développement, Laboratoire d'Etudes en Géophysique et Océanographie Spatiales, Toulouse, France.

Corresponding author: T. Qu, International Pacific Research Center, SOEST, University of Hawaii at Manoa, 1680 East-West Rd., Honolulu, Hawaii 96822, USA. (tangdong@hawaii.edu)

2169-9275/14/10.1002/2013JC009375

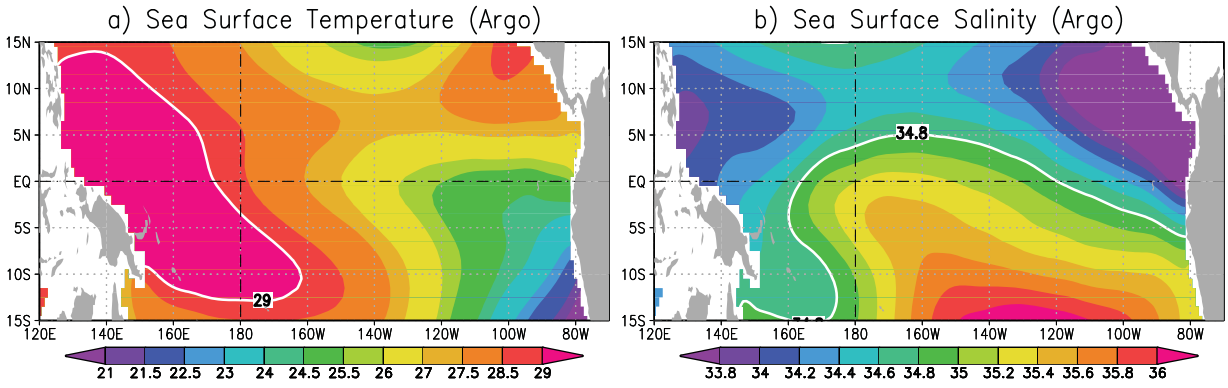

Figure 1. Long-term (January 2005 to July 2013) mean sea surface (a) temperature (°C) and (b) salinity (psu) from Argo. The thick white lines represent the 29°C isotherm in Figure 1a and 34.8 psu isohaline in Figure 1b, and the black dot-dashed lines show the equator and the international dateline.

events to a shallow mixed layer, the barrier layer favors the eastward displacement of the warm pool during the onset of El Niño [*Maes et al*., 2002]. In the absence of salinity stratification, the eastward displacement of the warm pool was reduced, which in turn led to a reduced El Niño or a return to the mean seasonal cycle of the model. These results seem to suggest that the barrier layer is a potentially important process influencing ENSO and merits careful consideration in climate research.

[6] The SSS and barrier layer variability in the equatorial Pacific has been investigated by previous studies, based on oceanographic cruise data, reconstructed salinity profiles, and Voluntary Observing Ship thermosalinograph measurements [e.g., *Lukas and Lindstrom*, 1991; *Sprintall and Tomczak*, 1992; *Rodier et al*., 2000; *Delcroix and McPhaden*, 2002; *Fujii and Kamachi*, 2003; *Maes et al*., 2002, 2004]. Recently, by combining available Argo data with the Tropical Atmosphere-Ocean/Triangle Trans-Ocean Buoy Network (TRITON) measurements, *Maes et al*. [2006] found a tight relationship between the SSS front and the eastern edge of the warm pool for the period 2002–2004. This relationship was updated later by *Bosc et al*. [2009] using Argo profiles for the 2000–2007 period. These studies also noted the presence of a thick barrier layer on the western side of the SSS front. Closely related to this thick barrier layer was an anomalously warm SST, showing additional evidence for the importance of salinity stratification in the region's ocean-atmosphere interaction and consequently, the zonal displacement of the warm pool.

[7] However, due to the lack of sufficient salinity observations, the relationship between the SSS variability and ENSO reported by these earlier studies has not been confirmed on time scales longer than several years, and a comprehensive description of the barrier layer variability within the interannual context is still lacking. The rapid advance in space-based remote sensing is revolutionizing ocean observations. In particular, the successful launch of Aquarius is providing a global observing capability of the ocean from space, generating near-synoptic SSS maps on global scale at a spatial resolution of ∼150 km every 7 days [*Lagerloef et al*., 2008]. The Aquarius data offer a unique opportunity, which has never been possible by conventional observations, to monitor the zonal displacement of the SSS front near the eastern edge of the western Pacific warm pool. The combined use of these SSS measurements with the ongoing collection of Argo profiles allows for further investigation of the relationship between the SSS and barrier layer variability, providing a potential monitoring of the barrier layer in the western equatorial Pacific using the SSS measurements from Aquarius. The results of the analyses are reported in this paper.

[8] The rest of the paper is organized as follows. A brief description of the data and method of analysis is presented in section 2. Comparison between the two data sets is first presented in section 3 to assess the quality of the Aquarius data in the equatorial Pacific. In section 4 we examine the zonal displacement of the SSS front along the equator, and in section 5 we discuss the stratification associated with this zonal displacement. The link of SSS and the barrier layer variability to ENSO is discussed in section 6. Results are finally summarized and discussed in section 7.

2. Data Description

[9] Two data sets are used in this study. One is the satellite-based SSS measurement from Aquarius, and the other is the in situ temperature/salinity profiles from Argo. The details of these two data sets are described below.

2.1. Aquarius

[10] The first validated, geographically gridded data set from Aquarius was recently released by the Ocean Salinity Science Team (http://podaac.jpl.nasa.gov/aquarius). This data set, called the Aquarius/SAC-D version 2.0 data, was based on measurements by three separate microwave radiometers that measure brightness temperature along an approximately 390 km wide swath using three separate beams with elliptical footprints of dimension 76 × 94 km, 84 × 120 km, and 96 × 156 km. The three nonoverlapping beams sample the ocean differently from one another geographically and with different incidence angles that affect the salinity retrieval algorithm. The retrieved SSS data for ascending and descending tracks were bias-adjusted and mapped to a 1° × 1° grid on a monthly time scale. The Aquarius mission requirement is that the global salinity root-mean-square error is no more than 0.2 psu on 150 × 150 km

and monthly average. As yet, the version 2 data set partially achieves this requirement. See *Lagerloef et al*. [2013] for more details. The smoothed monthly SSS data from all three beams for the period from August 2011 through July 2013 are used in the present analysis.

2.2. Argo

[11] In the last decade, a large number of Argo floats have been deployed, and more than 3500 of them are currently profiling over the global ocean (http://www.argo.ucsd.edu) [cf. *Argo Steering Team*, 1998]. The Argo floats record temperature and salinity at a vertical resolution of 1–5 m in the upper ocean and somewhat coarser at depth (25 m as the standard). The measurements extend from a typical top level around 5 m to about 2000 m depth. Based on these measurements, the Asian Pacific Data Research Center of the International Pacific Research Center, University of Hawaii, recently created a near-real-time, monthly temperature/salinity product for the global ocean at a 1° × 1° grid (data available at http://apdrc.soest.hawaii.edu/dods/public_data/Argo_Products/monthly_mean). This product has 26 (standard) levels in the upper 2000 m and spans from January 2005 to present. The vertical (standard) levels are the same as those used for the World Ocean Atlas [*Levitus*, 1982]. In preparing this data set, a variational analysis technique was used to interpolate temperature and salinity onto a 3-D spatial grid. For more details about this technique and other information about the data, see the documentation presented at http://apdrc.soest.hawaii.edu/projects/Argo/index.php. This SSS product provides a baseline data set to validate the Aquarius measurements. Its longer time series also allows us to investigate the SSS and barrier layer variability in the equatorial Pacific on the interannual time scale.

3. Comparison Between the Two Data Sets

3.1. Annual Mean

[12] Before proceeding to the analysis of Aquarius data, we first compare the data with Argo to assess their quality on the tropical Pacific basin scale. For the period from August 2011 to July 2013, the two data sets show similar SSS patterns (Figures 2a and 2b). Both the subtropical salinity maxima and the equatorial fresh water pools are well captured by Aquarius. Negative discrepancies with magnitude larger than 0.2 psu are mainly found along the eastern boundary (Figure 2c), where upwelling conditions prevail and where the Argo sampling is known to be less adequate. The largest positive discrepancies (∼0.2 psu) between the two data sets take place in the tropical Pacific along the Intertropical Convergence Zone (ITCZ) and the South Pacific Convergence Zone (SPCZ). These discrepancies are consistent with the region's high-precipitation conditions. As Aquarius only measures the skin surface salinity, its measurement can be easily affected by the fresh water lens resulting from the high precipitation in the region [*Lagerloef et al*., 2008; *Henocq et al*., 2010; *Boutin et al*., 2013]. In the Argo standard, the conductivity-temperature-depth (CTD) pump is usually turned off as the float ascends through the depth of 5 m to avoid possible contamination in the conductivity cell [*Riser et al*., 2008]. Thus, as a consequence, Argo profilers measure salinity around the 5 m depth that is assimilated to be the SSS, but it can be significantly different from the skin surface salinity in the precipitation dominated region like the western equatorial Pacific, as one can see from Figure 2c.

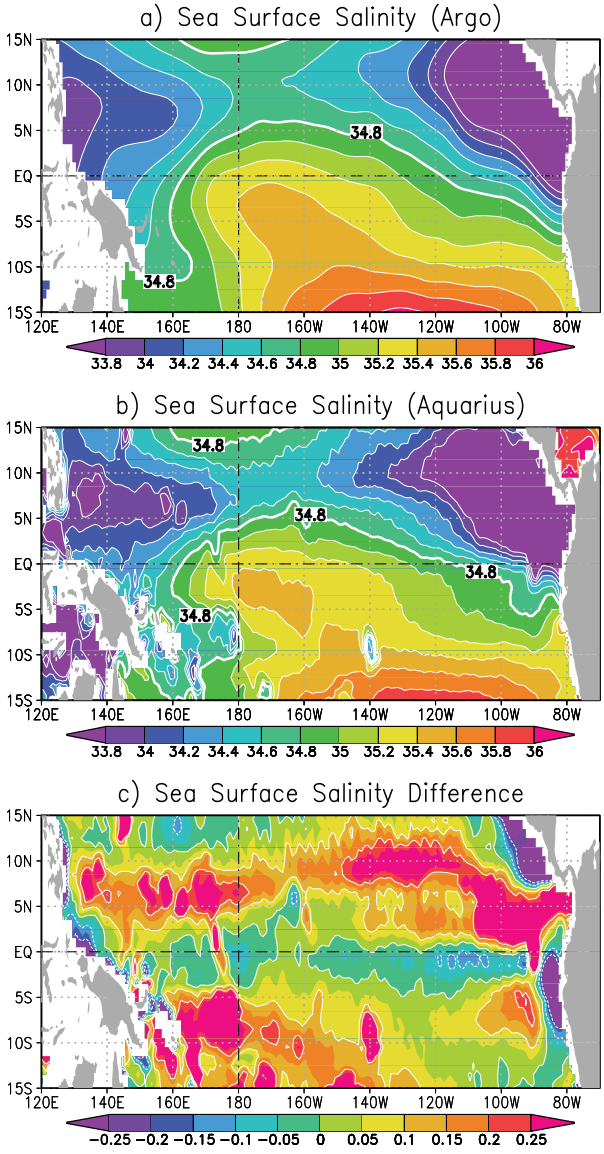

Figure 2. Mean sea surface salinity from (a) Argo and (b) Aquarius and (c) their difference (Argo-Aquarius) for the period August 2011 to July 2013. Unit is psu. The thick white lines in Figures 2a and 2b represent the 34.8 psu isohaline, and the black dot-dashed lines show the equator and the international dateline.

[13] Along the equator, the SSS discrepancies between the two data sets are generally small (<0.1 psu), well below the root-mean-square errors (∼0.2 psu) of the Aquarius data [*Lagerloef et al*., 2008]. The absence of structures along the equator indicates that errors of the Aquarius data are not sensitive to the presence of the warm pool and its front (Figure 2c). For the period of observation (August 2011 to July 2013), the mean SSS front from Aquarius as determined by the maximum zonal SSS gradient takes place at 169°E, showing a good agreement with that (174°E) from Argo. This result suggests that despite some uncertainties in the mean value (Figure 2c), Aquarius is able to capture the SSS

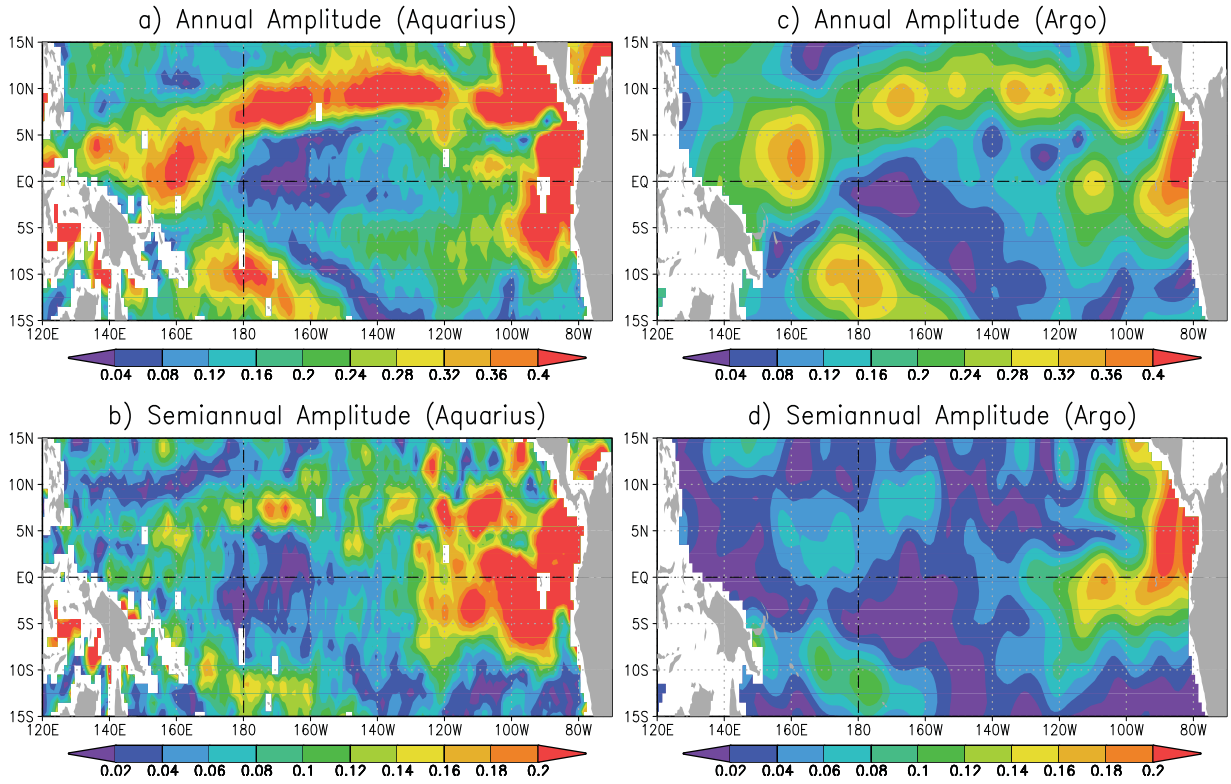

Figure 3. Amplitude of (top) annual and (bottom) semiannual variations of sea surface salinity from Aquarius (left) and Argo (right) for the period August 2011 to July 2013. Note that the amplitude of the color bars in the bottom panels has been divided by a factor of 3 from the color bars in the upper panels. The black dot-dashed lines show the equator and the international dateline. Unit is psu.

front along the equator, thus providing a potentially useful tool to monitor the eastern edge of the western Pacific warm pool. The details will be discussed in section 4.

3.2. Seasonal Cycle

[14] Harmonic analysis of Aquarius data provides a broad, consistent view of the SSS seasonal variation for the period from August 2011 to July 2013 in the tropical Pacific (Figure 3a). In general, the seasonal variation of SSS in the tropical Pacific is dominated by the annual cycle. A large portion of the tropical Pacific has an annual cycle of SSS less than 0.2 psu. The maximum amplitude ($\sim$0.6 psu) of SSS annual cycle takes place in the eastern equatorial Pacific, similar to what has been discussed for SST [e.g., *Kessler et al*., 1998]. Outside of the equator, a coherent band of SSS annual amplitude greater than 0.4 psu is seen, roughly coinciding with the ITCZ/SPCZ. Based on the World Ocean Atlas 1998 (WOA98), *Boyer and Levitus* [2002, Figure 3a] showed a similar pattern. They attributed the large SSS annual cycle in the tropical Pacific to the annual fluctuation of precipitation.

[15] For the same period of observation (August 2011 to July 2013), Argo shows essentially the same SSS annual cycle as Aquarius, with the tropical Pacific being dominated by a high-amplitude (>0.3 psu) band associated with the ITCZ/SPCZ (Figure 3c). Compared with those from Aquarius and WOA98 [*Boyer and Levitus*, 2002], the SSS annual cycle from Argo is somewhat weaker, presumably due to the insufficiency of sampling during the period of observation. By comparing the Aquarius SSS with Argo data and results from ocean models, *Song et al*. [2013] showed similar results for the global ocean, suggesting a global observing capability of the SSS annual cycle.

[16] The semiannual cycle is typically about two times weaker than the annual cycle (Figures 3b and 3d). In much of the region studied, the semiannual cycle from both data sets is less than 0.1 psu. Areas with SSS semiannual cycle greater than 0.2 psu include the eastern equatorial Pacific and the ITCZ/SPCZ in the tropics. So, the two data sets show essentially the same spatial patterns of the semiannual amplitude. A close inspection of these spatial patterns, however, indicates that Aquarius captures more small-scale features than Argo, which may reflect the difference in data coverage between the two data sets.

[17] Figure 4 shows the phase of SSS variation on both annual and semiannual time scales. Despite some quantitative discrepancies, the two data sets show essentially the same seasonal cycle in the tropical Pacific. Along the equator, SSS approaches its annual maximum in June/July east of the dateline and in March/April west of the dateline (Figures 4a and 4c). A phase difference of up to 3 months is also seen for the semiannual variation between the eastern and central equatorial Pacific (Figures 4b and 4d). No propagation signal is obvious along the equator, as can be derived from the nearly constant phase on both sides of the dateline. This result differs from those observed in the SST and sea surface height fields, in which propagation of both annual and semiannual variations has been identified [e.g.,

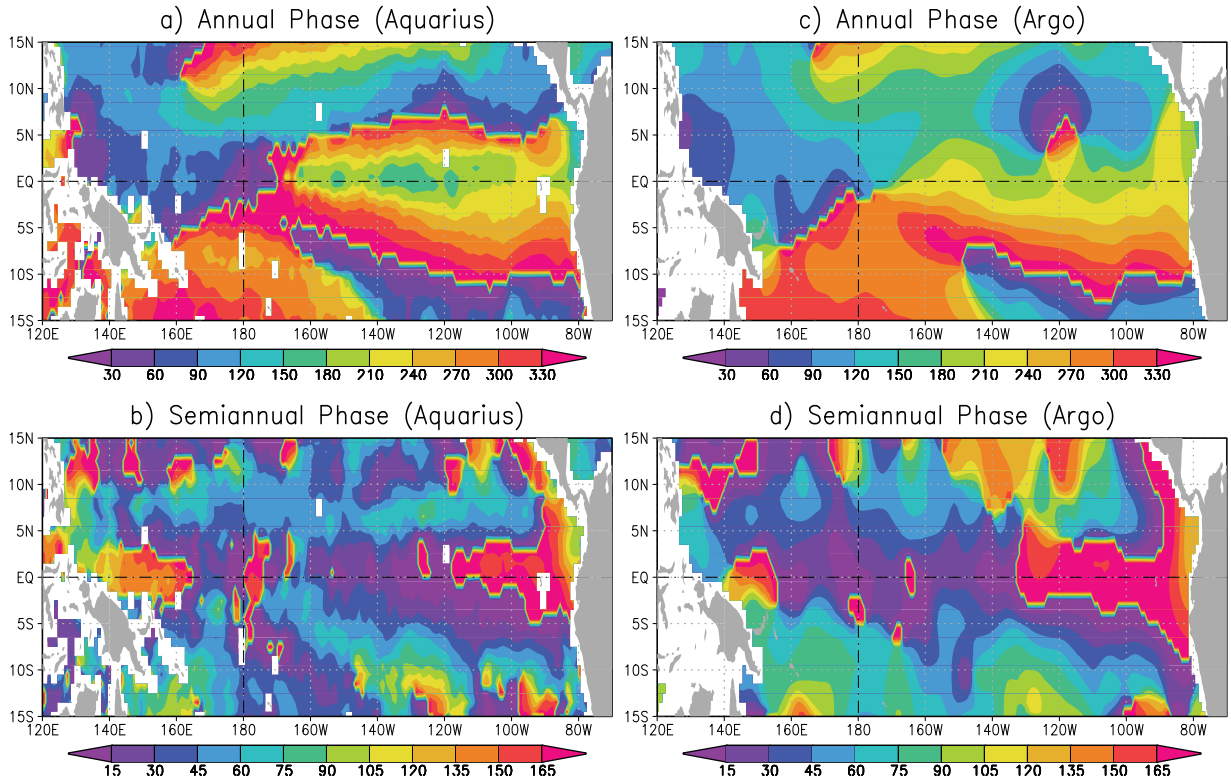

Figure 4. Phase of (top) annual and (bottom) semiannual variations, corresponding to the day of the year when SSS is maximum, from Aquarius (left) and Argo (right) for the period August 2011 to July 2013. The black dot-dashed lines show the equator and the international dateline.

Kessler, 1990; *Qu et al*., 2008]. The lack of propagation signal in the SSS field is not completely understood at present and needs to be investigated further.

[18] To demonstrate the SSS seasonal variation along the equator, Figure 5 shows the amplitude and phase of the annual and semiannual cycles averaged in the 3°S–3°N

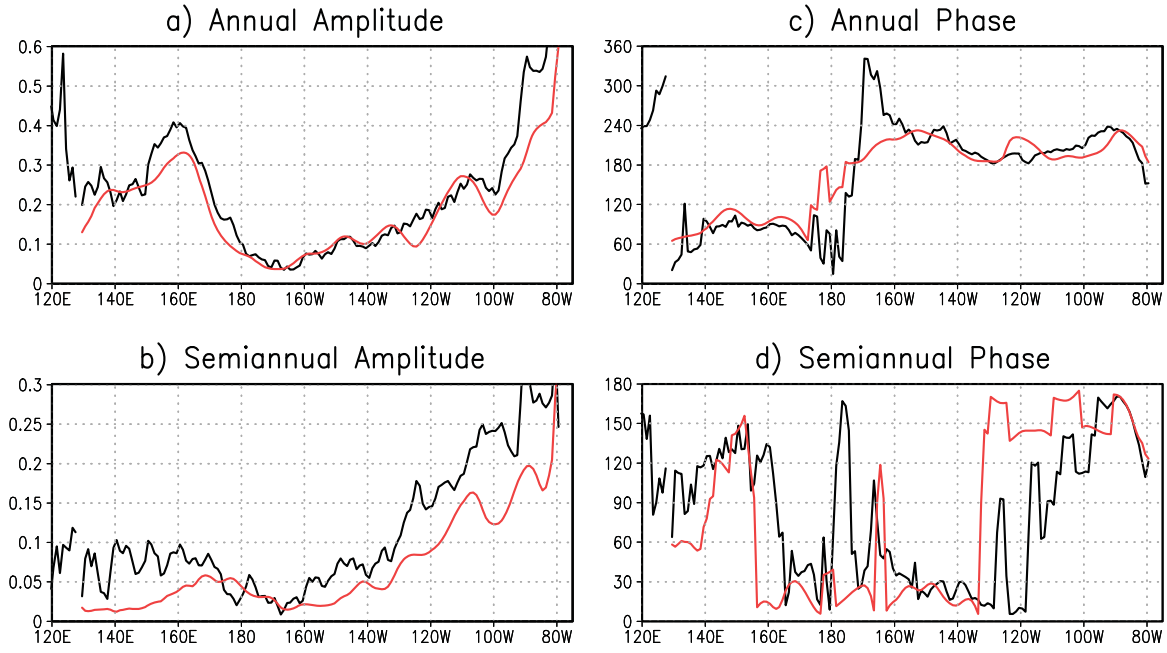

Figure 5. (top) Annual and (bottom) semiannual (left) amplitude and (right) phase of averaged sea surface salinity from Argo (red) and Aquarius (black) along the 3°S–3°N equatorial band. Note that the range of the semiannual amplitude is smaller than the range of the annual amplitude by a factor of 2. Units are psu on the left panels and days on the right panels.

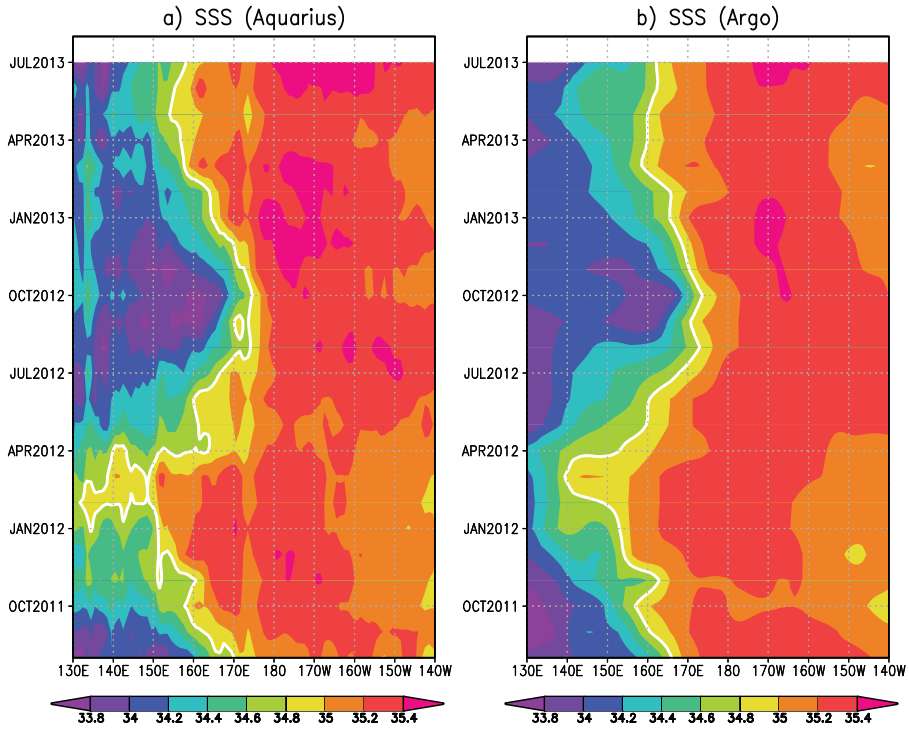

Figure 6. Time-longitude distribution of sea surface salinity along the 3°S–3°N equatorial band in the western central Pacific from (a) Aquarius and (b) Argo for the period August 2011 to July 2013. The white lines are the 34.8 psu isohalines representing the SSS front.

latitude band. The comparison between Aquarius and Argo is fairly good, with the amplitudes from the two data sets being almost identical. As has already been noted by previous studies [e.g., *Alory et al*., 2012], the SSS seasonal variation is largest in the eastern equatorial Pacific, where its annual and semiannual amplitudes exceed 0.6 and 0.3 psu, respectively. The amplitudes drop as we progress westward, falling below 0.2 psu for the annual cycle and below 0.1 psu for the semiannual cycle in the central equatorial Pacific. Both the annual and semiannual amplitudes increase in the western equatorial Pacific west of the dateline (Figures 5a and 5b).

[19] The phases of the SSS seasonal variation also show a good agreement between the two data sets (Figures 5c and 5d), except in the central equatorial Pacific near the dateline, where the phases of the annual cycle from Argo are much more smoothed than those from Aquarius. Some quantitative discrepancies are also evident for the semiannual variation. These include a phase difference of up to 3 months in the far eastern Pacific (east of 130°W) and a phase jump resolved by Aquarius in a narrow longitude band between 170°W and the dateline. These discrepancies are possibly related to the spatial sampling of the two data sets. The consistency of the two data sets is relatively good in the far western Pacific, suggesting that Aquarius is able to capture the western Pacific warm pool variation on both the annual and semiannual time scales.

4. Zonal Displacement of SSS Front

[20] To illustrate the zonal displacement of SSS front along the equator, Figure 6 shows the time-longitude distribution of SSS averaged over the latitude band between 3°S and 3°N for the period from August 2011 through July 2013. It is clearly shown that the zonal displacement of SSS front is well resolved by both data sets. Defined by the 34.8 psu isohaline, the SSS front is seen to migrate along the equator from month to month over a longitude band larger than 40°, consistent with the previous results reported by *Maes et al*. [2004]. During the 2011/2012 La Niña event, the SSS front moved westward to as far as about 140°E from its mean location near 170°E. For the period of observation (August 2011 to July 2013), the SSS front resolved by Aquarius is highly correlated with that resolved by Argo, with their correlation coefficient reaching 0.85 that satisfies the 99% confidence level by *t* test.

[21] It is worthwhile to note that with a global coverage of every 7 days, Aquarius is able to capture more features than Argo. In the region defined by 30°S–30°N and 120°E–80°W, approximately 3000 Argo profiles become available each month, which are roughly better than one profile per month in each 2° × 2° grid on the average. With such a sparse coverage, Argo cannot resolve all the detailed features of the SSS front. In this regard, Aquarius appears to offer a good opportunity to monitor the SSS front in the equatorial Pacific (Figure 6). This is very promising for further investigations as a longer time series of Aquarius data becomes available.

[22] The Argo data allow for further investigation of the zonal displacement of SSS front on the interannual time scale. Figures 7a and 7b show the time evolution of SST and SSS along the equator for the period from January 2005 to July 2013, respectively. From this figure one can see a good correspondence between the SST and SSS fields.

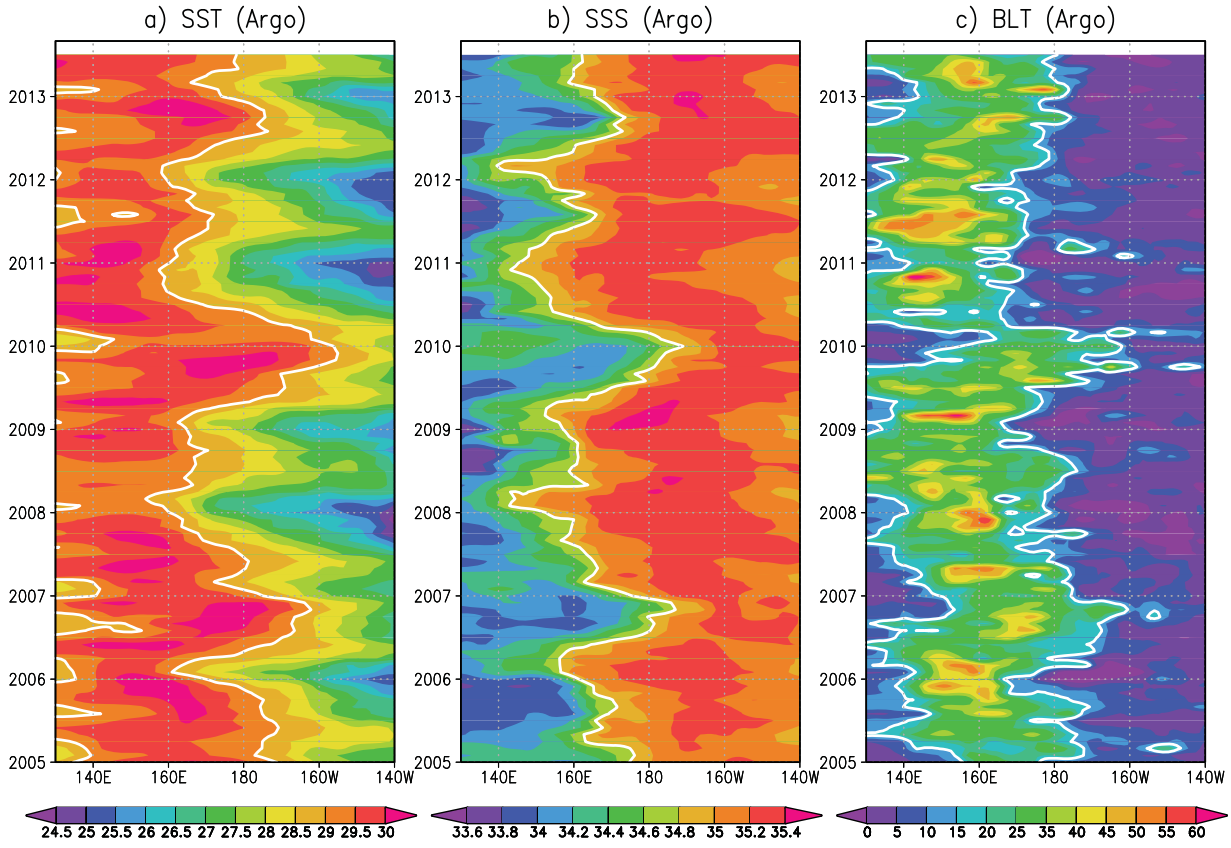

Figure 7. Time-longitude distribution of (a) sea surface temperature, (b) sea surface salinity, and (c) barrier layer thickness from Argo along the equator in the western central Pacific. Units are °C in Figure 7a, psu in Figure 7b, and m in Figure 7c. The white lines indicate the contours of 29°C, 34.8 psu, and 15 m, respectively.

The eastern edge of the warm pool, represented here by the 29°C isotherm, migrates from year to year against its mean location near 176°E. The SSS front, as indicated by the 34.8 psu isohaline, lies at 163°E in the mean, about 13° farther westward than the 29°C isotherm. This result is consistent with the previous studies suggesting that the presence of the SSS front is inside the 29°C warm pool [e.g., *Maes et al.*, 2004]. During the period of observation (January 2005 to July 2013), the SSS front and the eastern edge of the warm pool migrate in about the same phase, both showing a significant interannual variability (Figure 7).

[23] The correspondence of SSS front with the eastern edge of the warm pool has been investigated by earlier studies [e.g., *Picaut et al.*, 2001; *Maes et al.*, 2004, 2006; *Bosc et al.*, 2009]. The newly available Argo data allow us for a more detailed assessment of this relationship on the interannual time scale (Figure 8). During the period of observations (January 2005 to July 2013), the correlation between the two time series reaches as high as 0.9, satisfying the 99% significance level by *t* test (Table 1). This high correlation confirms that the eastern edge of the western Pacific warm pool is well characterized by the SSS front along the equator. As indicated by the heavy dotted red line in Figure 8, the SSS front from Aquarius shows consistent result with Argo for the period from August 2011 to July 2013.

5. Stratification

[24] Also included in Figure 7 is the time evolution of the barrier layer thickness (BLT) along the equator from Argo. In this study, we define the barrier layer in the same way as *Sprintall and Tomczak* [1992] by using a density difference from the surface value that is equivalent to a decrease (0.5°C) in temperature. Different methods can be used to define the barrier layer [e.g., *de Boyer Montegut et al.*, 2004], but the results remain essentially the same. In the mean, the barrier layer is thick in the western equatorial Pacific (Figure 9a). Its maximum thickness (>35 m) lies around 160°E along the equator, roughly on the western side of the SSS front (Figure 2). The mean BLT falls below 15 m at about 15° off the equator. Along the equator, a BLT front is seen near the dateline, and east of this front the BLT drops rapidly to less than 5 m. Given the vertical resolution (>5 m) of the Argo product, values less than 5 m are not shown and excluded from the discussion below. Standard deviations or root-mean-square variations of the BLT are also included in Figure 9b. In the equatorial Pacific, the largest (>15 m) BLT variability occurs near the dateline, roughly coinciding with the mean BLT front (Figure 9a). The zonal migration of thick barrier layer is apparently responsible for this large BLT variability. Variability near 160°E, where the mean BLT exceeds 30 m, is relatively weak (~10 m), suggesting that most of the mean

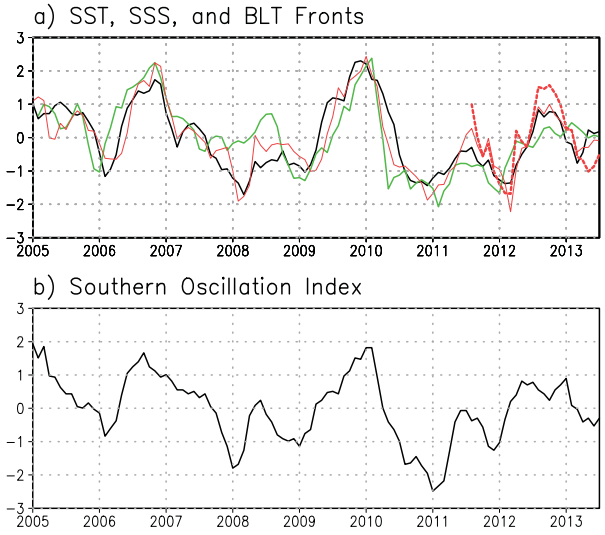

Figure 8. (a) Time series of the eastern edge of the warm pool (black), SSS front (red), and thick barrier layer (green) compared with (b) the Southern Oscillation Index. The heavy dotted red line in Figure 8a indicates the SSS front measured by Aquarius for the period from August 2011 through July 2013. Here the eastern edge of the warm pool, SSS front, and thick barrier layer are represented by the contours of 29°C, 34.8 psu, and 15 m, respectively. All time series are normalized by their respective standard deviations. The SOI in Figure 8b has been multiplied by −1 before plotting.

BLT features shown in Figures 7c and 9a for the equatorial Pacific are robust.

[25] Over much of the region studied, the BLT annual cycle is weaker than 6 m (Figure 10a). In the equatorial region, the annual amplitude exceeds 8 m near the coast of New Guinea and falls below 2 m around 160°E. It then increases toward the east, approaching its maximum (>8 m) at about 5° off the equator near the dateline. Interestingly, the annual amplitude near the dateline is actually very small (<4 m) on the equator (Figure 10a), which only explains about a quarter of the total (>16 m) variability there (Figure 9b). The semiannual cycle of the BLT (Figure 10b) shows a similar pattern as the annual cycle (Figure 10a), while its amplitude is about two times smaller. In general, the BLT has a tendency to follow the SSS seasonal cycle (Figures 4c and 10c). In the western equatorial Pacific, the SSS reaches its annual maximum in March/April (Figure 4c), which is in phase with the E-P annual fluctuation [e.g., *Boyer and Levitus*, 2002]. This SSS annual maximum is consistent with a BLT annual minimum in much of the western equatorial Pacific (Figure 10c), suggesting a good correspondence between SSS and surface stratification. Similar correspondence is also evident for the semiannual variation (Figures 4d and 10d).

[26] While displaying a weak seasonal cycle, most of the BLT variability along the equator is due to the zonal displacement of the thick barrier layer on the interannual time scale. For the period of observation, the zonal displacement of the thick barrier layer concurs with that of the eastern edge of the warm pool in almost all the cases (Figure 7). Its year-to-year zonal displacement along the equator can exceed 4000 km. Using the 15 m contour as its eastern edge (Figure 7c), the presence of the thick barrier layer is highly correlated with the 29°C isotherm and 34.8 psu isohaline (Figure 8), and their overall correlation reaches 0.76 and 0.79, respectively (Table 1). Note that the 15 m thickness of the barrier layer is above the root-mean-square errors of the BLT (Figure 9b) and is significant in the view of sensitivity for the background mean state in the western equatorial Pacific [e.g., *Maes and Belamari*, 2011]. Following the tilting/shearing mechanism suggested by *Cronin and McPhaden* [2002], this result seems to suggest that the zonal displacement of the SSS front can affect the surface stratification and consequently, the presence of the thick barrier layer in the western equatorial Pacific. The processes that maintain this relationship are not completely clear to us. As a dominant climate mode of the region, ENSO likely plays a role [e.g., *Picaut et al*., 1997]. The details are discussed below.

6. Link to ENSO

[27] Following the pioneering works of *Lindstrom et al*. [1987] and *Lukas and Lindstrom* [1991], the barrier layer variability in the western Pacific has been investigated by many studies. Based on CTD measurements along 165°E from 1984 to 1988, *Delcroix et al*. [1992] reported that the barrier layer in the western Pacific was destroyed during episodes of eastward surface flow and equatorial upwelling driven by easterlies. Later studies focused on the barrier layer variability on the interannual time scale [e.g., *Ando and McPhaden*, 1997; *Maes*, 2000; *Delcroix and McPhaden*, 2002; *Cronin and McPhaden*, 2002] and found a clear correspondence between the barrier layer variability and ENSO [e.g., *Fujii and Kamachi*, 2003; *Maes et al*., 2002, 2005, 2006]. Based on the early development of the Argo data, *Bosc et al*. [2009] noted that the barrier layer in the western equatorial Pacific represents a quasi-permanent feature for both El Niño and La Niña events. But the precise relationship between the BLT and ENSO was not determined by these earlier studies due to the short period of their observations.

[28] The correspondence between the barrier layer variability and ENSO is supported by the present analysis. In Figure 7, we see eastward displacements of the thick barrier layer during the 2006/2007 and 2009/2010 El Niño events and westward displacements during the 2007/2008, 2010/

Table 1. Correlations Among the Eastern Edge of the Warm Pool (WP) (29°C), SSS Front (34.8 psu), Thick Barrier Layer (BL) (15 m) From Argo, and SOI for the Period From January 2005 to July 2013[a]

Correlation	Eastern Edge WP	SSS Front	Thick BL	SOI
Eastern edge WP	1.00 (0)	0.90 (0)	0.76 (1)	−0.82 (1)
SSS front	0.90 (0)	1.00 (0)	0.79 (1)	−0.84 (1)
Thick BL	0.76 (−1)	0.79 (−1)	1.00 (0)	−0.81 (0)
SOI	−0.82 (−1)	−0.84 (−1)	−0.81 (0)	1.00 (0)

[a]All correlations satisfy the 99% confidence level. Numbers in the brackets indicate the time (in months) that variables in the first column lag those in the first row.

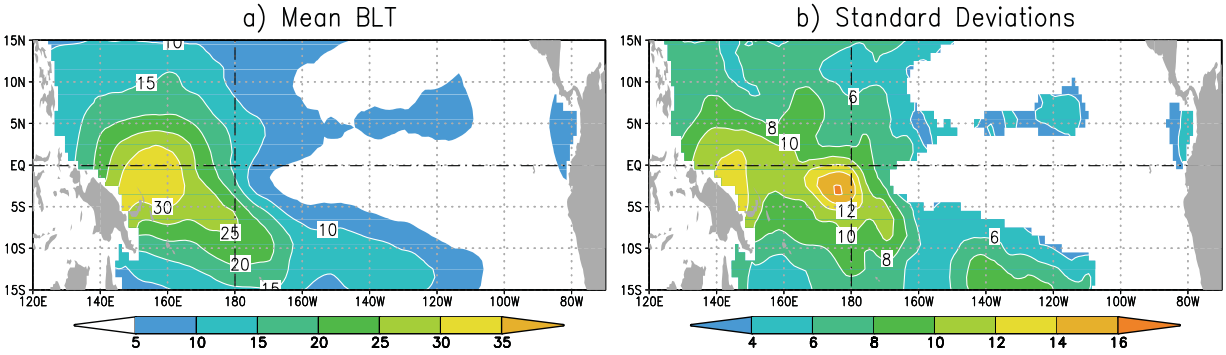

Figure 9. (a) Time mean and (b) standard deviations of the barrier layer thickness for the period from January 2005 to July 2013 from Argo. The black dot-dashed lines show the equator and the international dateline. The contour intervals are set every 5 m for BLT and 2 m for the standard deviations.

2011, and 2011/2012 La Niña events. These zonal displacements are in phase with those of the eastern edge of the warm pool and the SSS front along the equator as indicated by the 29°C isotherm and 34.8 psu isohaline, respectively (Figures 7a and 7b). During the period of observation, these time series corresponded well with ENSO (Figure 8), with their correlation with the Southern Oscillation Index (SOI) all exceeding 0.80 (Table 1). During the 2009/2010 El Niño event, for example, the thick (>15 m) barrier layer moved eastward to about 160°W, and in the same time both the eastern edge of the warm pool and the SSS front reached their easternmost positions along the equator. Interestingly, the thick barrier layer appears to lead both the eastern edge of the warm pool and the SSS front along the equator by 1 month (Table 1). The implication of this result is that the response of the western equatorial Pacific to ENSO first occurs in the subsurface. Then the corresponding changes in subsurface stratification may further affect the sea surface and play a role in the zonal displacement of the warm pool. The existing data are apparently not sufficient for a detailed investigation of this phase difference, and we will leave it for future studies.

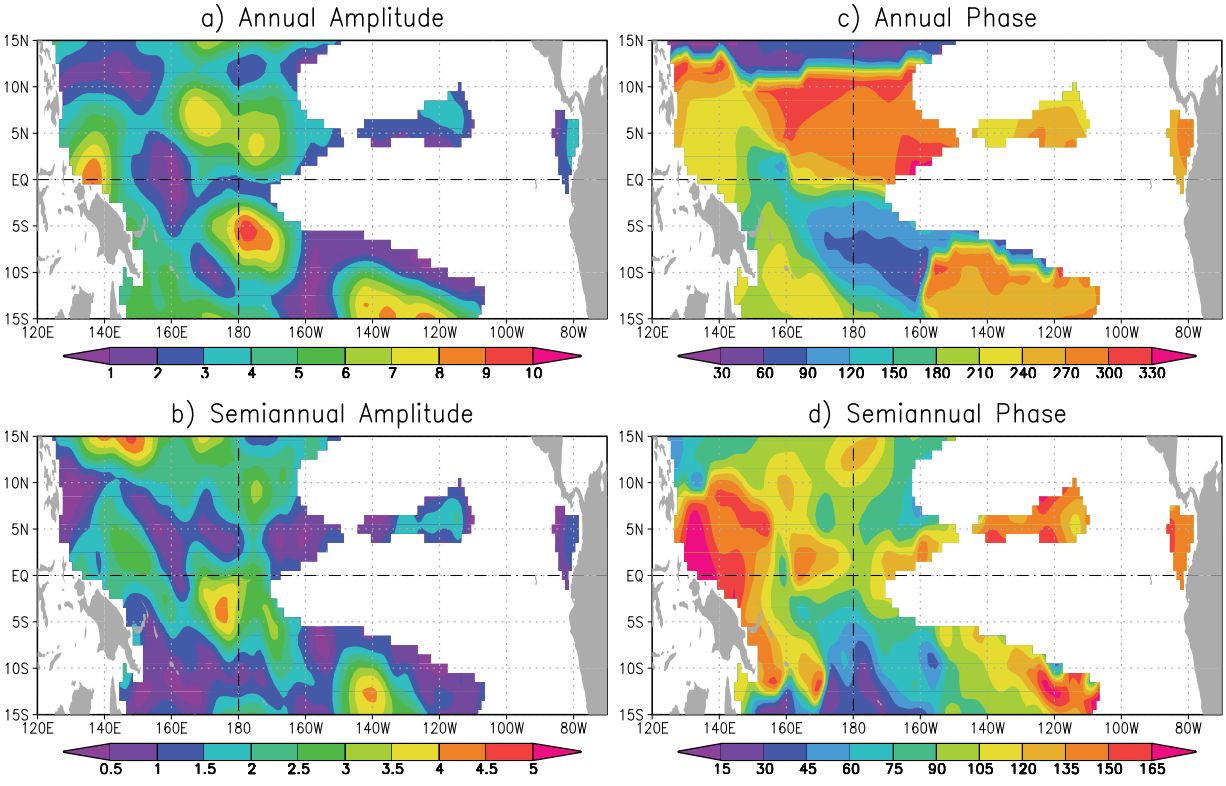

Figure 10. (top) Annual and (bottom) semiannual (left) amplitude and (right) phase of the BLT (m) variation from Argo for the period August 2011 to July 2013. Note that the amplitude of the color bars in the bottom panels has been divided by a factor of 2. The phase indicates the day of the calendar year when BLT reaches its maximum. The black dot-dashed lines show the equator and the international dateline.

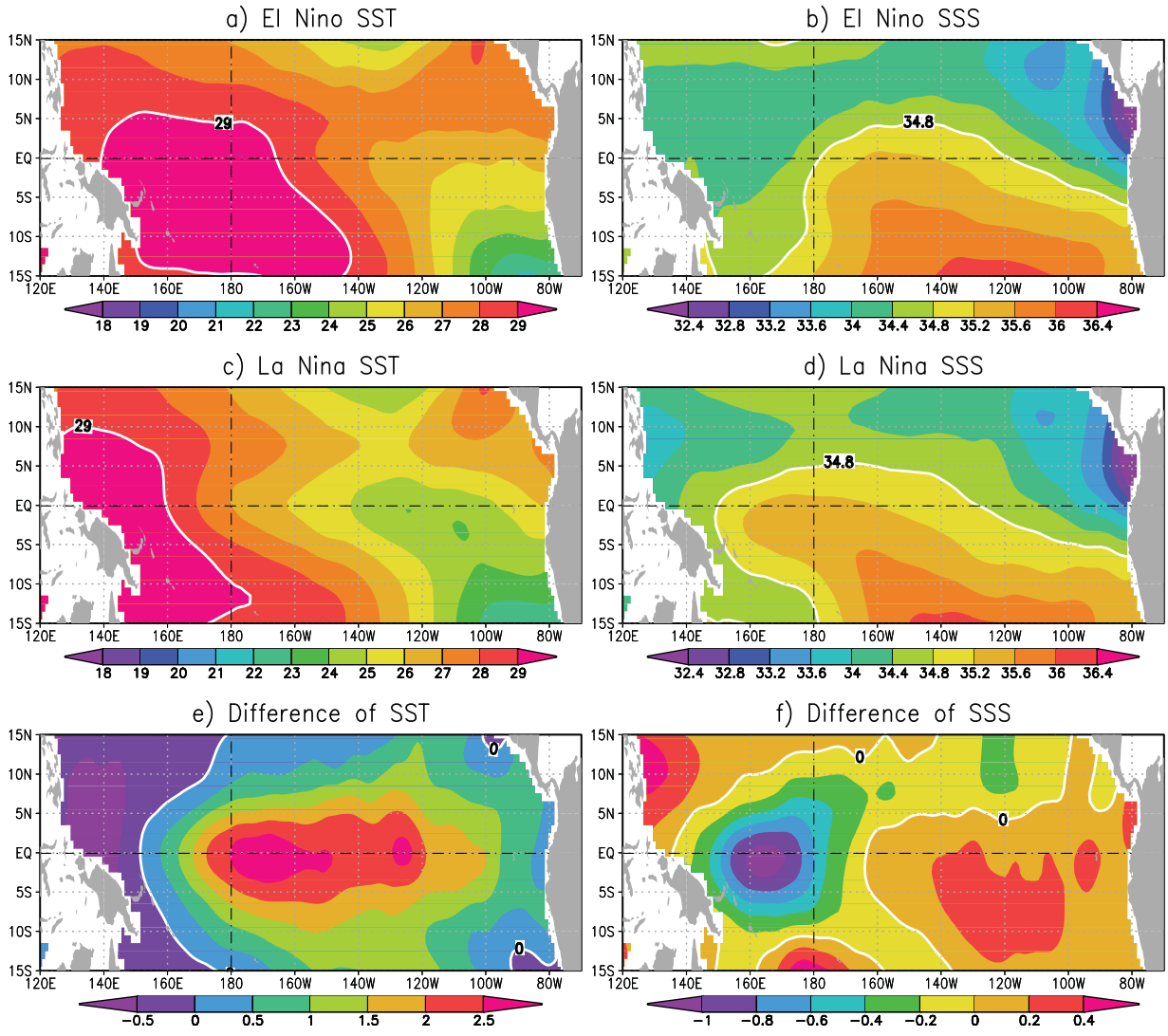

Figure 11. Composites of (left) sea surface temperature in °C and (right) salinity in psu during the mature phase of (top) El Niño, (middlre) La Niña, and (bottom) their differences in the tropical Pacific. The composite of El Niño conditions includes 12/2006–02/2007 and 12/2009–02/2010, and the composite of La Niña conditions includes12/2007–02/2008, 12/2010–02/2011, and 12/2011–02/2012. The solid white lines represent the 29°C isotherm, the 34.8 psu isohaline, and the zero isoline. The black dot-dashed lines show the equator and the international dateline.

[29] To further illustrate how the eastern edge of the warm pool, the SSS front, and the thick barrier layer are related to ENSO, we conduct a composite analysis of the two El Niño events (2006/2007 and 2009/2010) and three La Niña events (2007/2008, 2010/2011, and 2011/2012) that took place during the period of observation (Figure 11). The SOIs during these events all exceeded one standard deviation of its variability (Figure 8b). During El Niño conditions, as one has already known, SST gets warmer in the central and eastern equatorial Pacific, while SSS gets fresher in the western equatorial Pacific, roughly, between 160°E and the dateline. The situation is reversed during La Niña conditions [e.g., *Singh et al*., 2011]. Corresponding to these SST and SSS variations, the mixed layer depth also changes from El Niño to La Niña conditions (Figure 12). The differences between the two composite events show a shallower mixed layer west of the dateline and a deeper mixed layer east of it (Figure 12e). Most of the BLT variations are confined in the western central equatorial Pacific, roughly, to the west of 160°W (Figure 12f). During El Niño conditions, the barrier layer generally gets thicker in the longitude band between 160°E and 160°W on the equator but becomes thinner west of 160°E off the equator.

[30] Figure 13 shows the composite wind stress and P-E from the National Centers for Environmental Prediction (NCEP)/National Center for Atmospheric Research Reanalysis Project [*Kalnay et al*., 1996]. As noted by many previous studies mentioned above, the largest wind stress differences between El Niño and La Niña are the westerly wind anomalies in the western equatorial Pacific (Figure 13e). Associated with these westerly wind anomalies are positive P-E anomalies (Figure 13f). The spatial pattern of the positive P-E anomalies essentially follows the ITCZ and SPCZ, with their maximum values (>10 mm d^{-1})

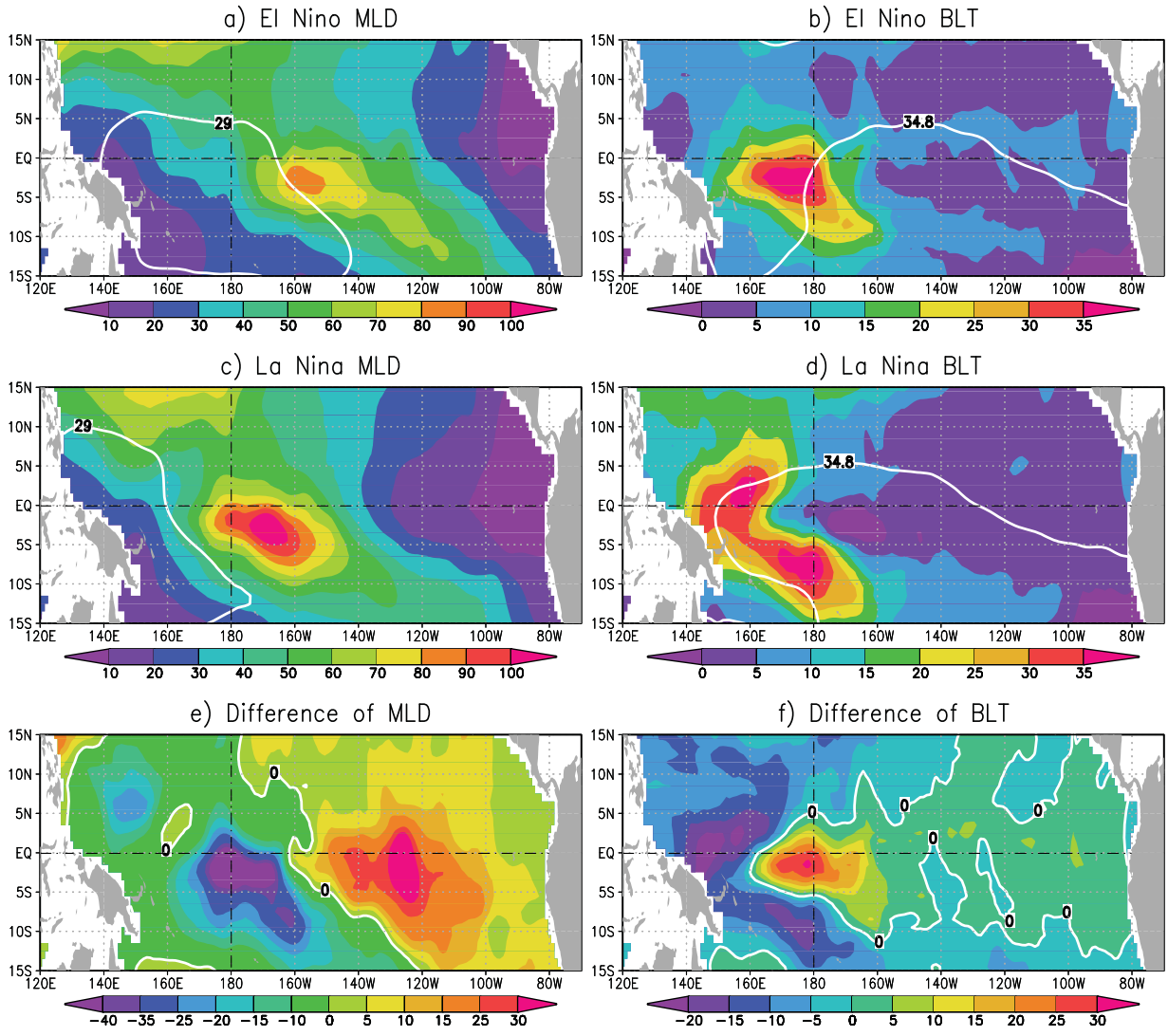

Figure 12. Same as Figure 11 except for (left) mixed layer depth and (right) barrier layer thickness. Unit is meters.

lying between 160°E and 170°E near the equator. In the eastern equatorial Pacific, the P-E anomalies are weak, and they are generally positive north of the equator and negative south of it. The P-E anomalies in the eastern equatorial Pacific are inconsistent with the SSS anomalies, which are mostly positive east of the dateline (Figure 11). This result clearly demonstrates that P-E is not the only process influencing SSS. In addition to the P-E anomalies, ocean dynamics also plays a significant role in generating the SSS variability [e.g., *Johnson et al*., 2002].

[31] Regarding the formation of thick barrier layer, several processes may be at work [*Bosc et al*., 2009]. For example, the eastward shift of heavy rainfall associated with the westerly wind anomalies during El Niño (Figures 13a and 13b) corresponds with an eastward shift of the warm pool by up to 2000 km (Figures 11a and 11b) relative to its mean position (Figure 1a). The eastward shift of the warm pool then generates a shallower isohaline surface layer in the western equatorial Pacific (Figure 12a), which in turn may directly contribute to the presence of the thick barrier layer there (Figure 12b) [e.g., *Sprintall and Tomczak*, 1992]. At the same time, the meridional wind anomalies north of the equator (Figure 13e) force the surface freshwater near the ITCZ (Figure 11b) to flow equatorward [e.g., *McPhaden et al*., 1992]. These processes, together with the surface water convergence forced by the westerly wind bursts along the equator [e.g., *Cronin and McPhaden*, 2002], may enhance the surface stratification, providing a favorable condition for the eastward displacement of the thick barrier layer. The situation is reversed during La Niña conditions.

[32] Figure 14 shows the temperature and salinity along the equator to further illustrate the differences in vertical structures between the two events (Figure 14). Based on CTD measurements collected by three oceanographic cruises, *Maes* [2008] noticed an increasing east-west gradient in salinity stratification within the isothermal layer, with the higher values lying to the west of the eastern edge of the warm pool. This east-west gradient in salinity stratification is also well captured by Argo (Figure 14), shifting from about 160°E during El Niño (Figure 14b) to the coast of New Guinea (west of 130°E) during La Niña (Figure

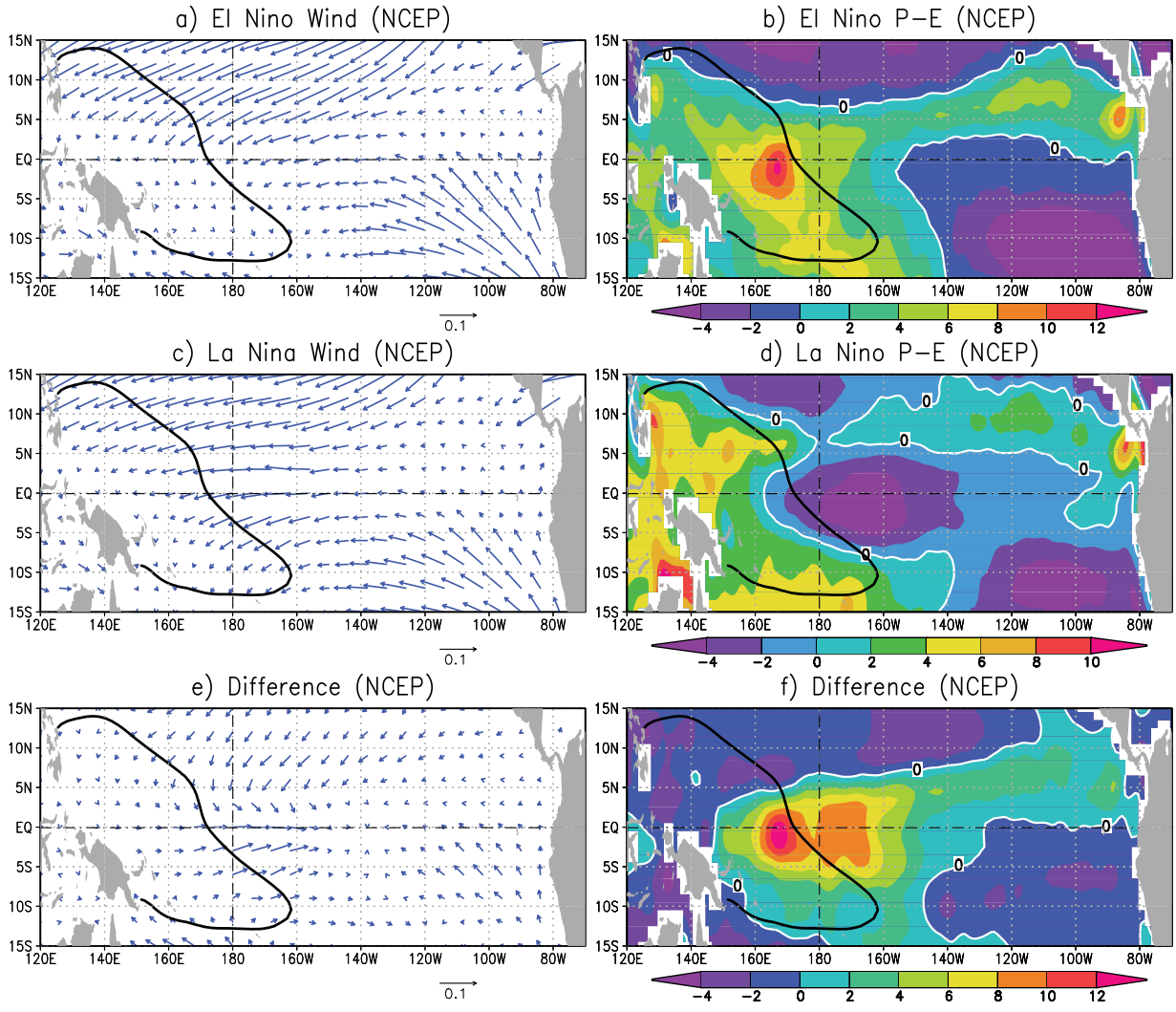

Figure 13. Same as Figure 11 except for (left) wind stress and (right) precipitation minus evaporation (P-E) from NCEP reanalyses. The black lines indicate the mean 29°C isotherm. Units are N m^{-2} for wind stress and mm d^{-1} for P-E. The black dot-dashed lines show the equator and the international dateline.

14d). In both cases, the maximum salinity stratification is confined above the thermocline (black solid lines), within the density range less than 22.5 kg m^{-3}. During El Niño conditions, the eastern edge of the warm pool as indicated by the 29°C isotherm reaches about 170°W on the equator (Figure 14a). Immediately to the west of the eastern edge of the warm pool is a salinity front, whose maximum zonal gradient coincides with the 34.8 psu isohaline near the dateline (Figure 14b). A thick (>15 m) barrier layer concurs with this salinity front and covers a longitude band roughly between 160°E and170°W. During La Niña conditions, as the eastern edge of the warm pool approaches its western most position near 160°E, the salinity front shifts westward by nearly 3000 km from its El Niño condition, which in turn results in a westward displacement of the thick barrier layer (Figures 14c and 14d).

[33] What we would like to emphasize here is the presence of minimum stratification lying to the east of the western Pacific warm pool, where mixed layer depth can reach as deep as 100 m (Figure 14a). Closely related to this minimum stratification is the vertical entrainment of high-salinity (>35.2 psu) water from below along density surfaces near 22.5 kg m^{-3} (Figure 14b). This high-salinity water represents a mix of subtropical water from both hemispheres [e.g., *Lindstrom et al*., 1987; *Bingham and Lukas*, 1995; *Qu et al*., 1999]. During El Niño conditions, the thermocline shoals in the western equatorial Pacific and deepens in the central and eastern parts of the basin. These changes generate large temperature and salinity anomalies along the equator, with higher values lying around the thermocline, and as a consequence, potential density increases in the western and decreases in the central and eastern equatorial Pacific by up to 1 kg m^{-3} from El Niño to La Niña (Figures 14e and 14f). Such large density changes are also evident in the TRITON mooring data [e.g., *Hasegawa et al*., 2013], suggesting an eastward transport of warm and low-salinity water in the upper ocean. With the deepening of the thermocline in the central equatorial Pacific, the vertical entrainment of high-salinity water is much reduced during El Niño conditions, and its location moves to about

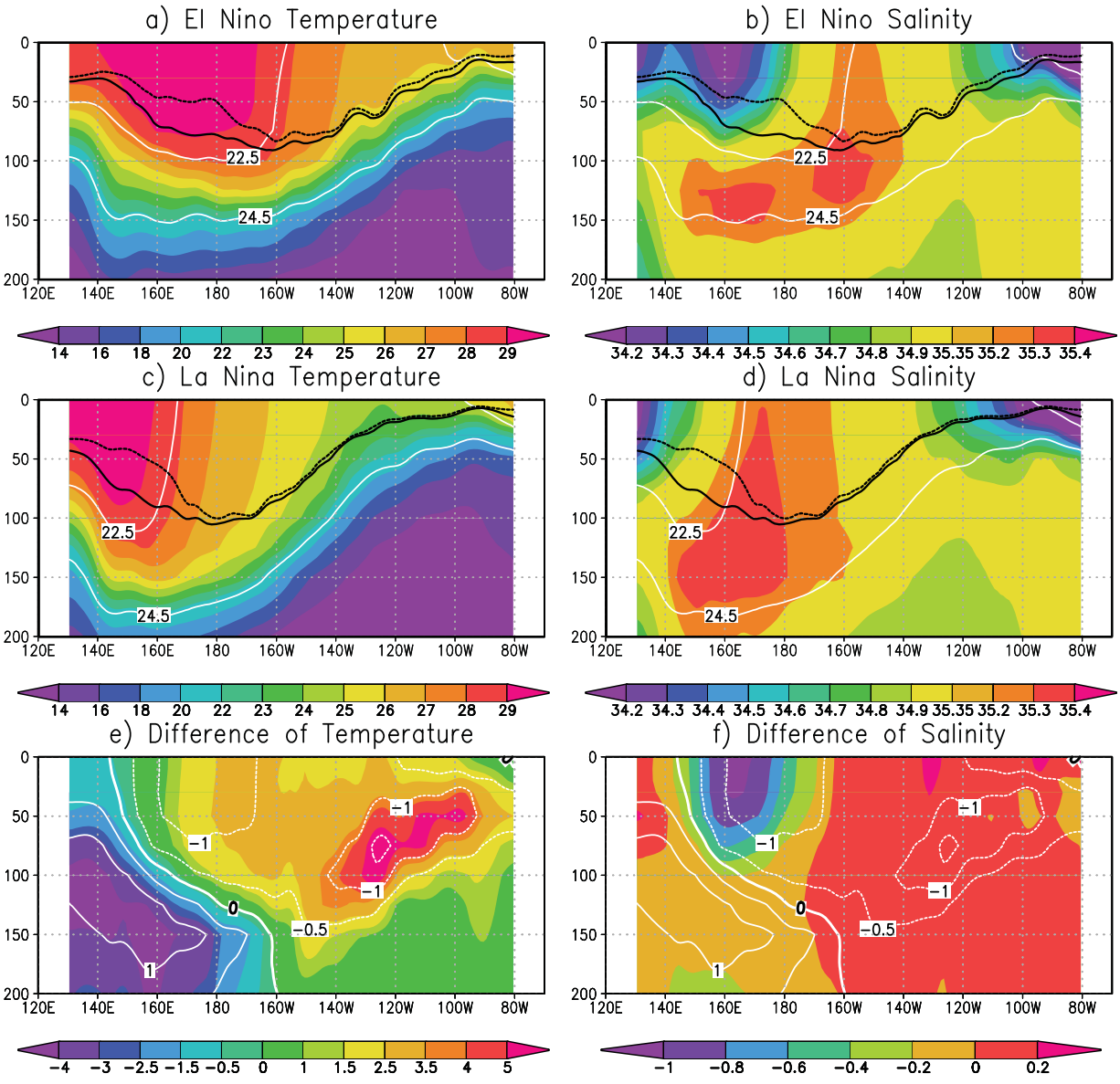

Figure 14. Same as Figure 11 except for vertical distributions of (left) temperature and (right) salinity along the equator from Argo. The white contours indicate potential density, and the black lines represent the top of the thermocline (solid) and the base of the mixed layer (dotted). The units are °C for temperature, psu for salinity, and kg m^{-3} for potential density.

160°W along the equator (Figure 14b). During La Niña conditions, the entrainment of high-salinity water reaches its western most position near 170°E, and high-salinity (>35.4 psu) water is seen to extend all the way to the sea surface, suggesting enhanced subsurface influence (Figure 14d). Since the high-salinity water is of subtropical origin, its entrainment in the equatorial Pacific cannot be forced by local processes (e.g., P-E and wind) alone. Then, what is responsible for the zonal displacement of the SSS front and its associated thick barrier layer? How much of this zonal displacement is due to the entrainment of high-salinity water from below? These questions will be addressed by future studies using results from high-resolution ocean general circulation models.

7. Summary and Discussion

[34] Using recently available Aquarius and Argo data, this study provides a detailed description of the SSS and barrier layer variability in the equatorial Pacific. For the period of Aquarius observation (August 2011 to July 2013), the two data sets agree reasonably well in both the mean value and seasonal variability. In the mean, the largest discrepancies between the two data sets take place along the ITCZ and SPCZ. These discrepancies may represent the differences between the skin surface salinity and surface layer salinity. They may also represent the insufficiency of Argo sampling in resolving high-frequency fluctuations of SSS fronts [e.g., *Juza et al.*, 2012; *Song et al.*, 2013]. For example, Aquarius can clearly see the Tropical Instability

Wave fronts, while Argo is less effective [*Lee et al*., 2012]. As the ITCZ/SPCZ region is dominated by low-wind, high-precipitation conditions, the fresh water lens resulting from heavy rainfall may not be mixed away immediately, and as a consequence, the skin surface salinity measured by Aquarius may be significantly lower than that at 5 m depth from Argo floats. To our knowledge, the Aquarius Ocean Salinity Science Team is deploying more Argo floats with the capacity of skin surface salinity measurement, so that the Aquarius data can be better calibrated and validated. Similar efforts are also being made with drifter buoys [e.g., *Reverdin et al*., 2013].

[35] Both the Aquarius and Argo data can nicely resolve the SSS front along the equator. With a better resolution in both space and time, Aquarius is able to capture more detailed features of the SSS front than Argo, demonstrating its observing capacity of the western Pacific warm pool, while the longer time series of Argo data allows for a more precise investigation of its interannual variation. The Argo data also provide information on stratification of the western Pacific warm pool, of which an important feature is the presence of a thick (>15 m) barrier layer. With these Argo data, we are able to show that the thick barrier layer in the equatorial Pacific varies both seasonally and interannually. While displaying a weak seasonal variability, the thick barrier layer can move eastward by up to 4000 km during an El Niño event. As Aquarius continues to provide the time series of ocean surface salinity, we anticipate that the SSS front, the thick barrier layer, and the eastern edge of the western Pacific warm pool will become adequately resolved, and their relationship with ENSO will be better understood.

[36] The formation mechanism of the thick barrier layer in the equatorial Pacific has been discussed by many earlier studies. In addition to the surface processes proposed by these earlier studies, we emphasize the effect of high-salinity water from below, representing a mix of subtropical water from both hemispheres. Based on available Argo and TRITON data, *Hasegawa et al*. [2013] noted that precipitation and salinity changes are not consistent in some parts of the equatorial Pacific. Apparently, local effect of precipitation cannot explain the salinity changes there. They speculated that oceanic advection and upwelling are probably of more importance in such regions. In a recent study using a simulate passive tracer, *Qu et al*. [2013] further demonstrated that a large portion of the high-salinity South Pacific tropical water makes its way into the equatorial region in the depth of the thermocline. From there, some of this water mass is entrained into the surface mixed layer in the central equatorial Pacific. The vertical entrainment of high-salinity water in the equatorial Pacific depends on local Ekman pumping and basin-scale gyre circulation, both of which have a strong ENSO signature. So, one may have reason to believe that the vertical entrainment of high-salinity water from below is also governed by ENSO, and its interannual variability may directly contribute to the zonal displacement of the SSS front and its associated thick barrier layer. The 1 month lead of the thick barrier layer to the eastern edge of the warm pool and the SSS front along the equator could be regarded as evidence for this subsurface influence. How this subsurface influence plays a role in the ENSO cycle and in particular, in the development of Central Pacific El Niño or Modoki [e.g., *Yu and Kao*, 2007; *Takahashi et al*., 2011] is an interesting topic for future studies.

[37] **Acknowledgments.** T. Qu was supported by NSF through grant OCE11-30050 and by NASA as part of the Aquarius Science Team investigation through grant NNX12AG02G. Y. T. Song was supported by the Jet Propulsion Laboratory, California Institute of Technology, under contracts with NASA. C. Maes is supported by IRD. The authors are grateful to N. Schneider and I. Fukumori for useful discussion on the topic, to K. Yu for assistance in processing the Aquarius data, and to two anonymous reviewers for valuable comments on this manuscript. School of Ocean and Earth Science and Technology contribution number 9054 and International Pacific Research Center contribution IPRC-1033.

References

Alory, G., C. Maes, T. Delcroix, N. Reul, and S. Illig (2012), Seasonal dynamics of sea surface salinity off Panama: The far eastern Pacific fresh pool, *J. Geophys. Res.*, *117*, C04028, doi:10.1029/2011JC007802.

Ando, K., and M. J. McPhaden (1997), Variability of surface layer hydrography in the tropical Pacific Ocean, *J. Geophys. Res.*, *102*, 23,063–23,078, doi:10.1029/97JC01443.

Argo Steering Team (1998), On the design and Implementation of Argo—An initial plan for the global array of profiling floats, *Int. CLIVAR Proj. Off. Rep., 21*, 32 pp.

Bingham, F. M., and R. Lukas (1995), The distribution of intermediate water in the western equatorial Pacific during January-February 1986, *Deep Sea Res., Part II*, *42*, 1545–1573.

Bosc, C., T. Delcroix, and C. Maes (2009), Barrier layer variability in the western Pacific warm pool from 2000 to 2007, *J. Geophys. Res.*, *114*, C06023, doi:10.1029/2008JC005187.

Boutin, J., N. Martin, G. Reverdin, X. Yin, and F. Gaillard (2013), Sea surface freshening from SMOS and ARGO salinity: Impact of rain, *Ocean Sci.*, *9*, 183–192, doi:10.5194/os-9-183-2013.

Boyer, T. P., and S. Levitus (2002), Harmonic analysis of climatological sea surface salinity, *J. Geophys. Res.*, *107*(C12), 8006, doi:10.1029/2001JC000082.

Chen, D. (2004), Upper ocean response to surface momentum and freshwater fluxes in the western Pacific warm pool, *J. Trop. Oceanogr.*, *23*, 1–15.

Cronin, M. F., and M. J. McPhaden (2002), Barrier layer formation during westerly wind bursts, *J. Geophys. Res.*, *107*(C12), 8020, doi:10.1029/2001JC00117.

de Boyer Montegut, C., G. Madec, A. S. Fischer, A. Lazar, and D. Iudicone (2004), Mixed layer depth over the global ocean: An examination of profile data and a profile-based climatology, *J. Geophys. Res.*, *109*, C12003, doi:10.1029/2004JC002378.

Delcroix, T., and M. J. McPhaden (2002), Interannual sea surface salinity and temperature changes in the western Pacific warm pool during 1992–2000, *J. Geophys. Res.*, *107*(C12), 8002, doi:10.1029/2001JC000862.

Delcroix, T., G. Eldin, M.-H. Radenac, J. Toole, and E. Firing (1992), Variation of the western equatorial Pacific Ocean, 1986–1988, *J. Geophys. Res.*, *97*, 5423–5445, doi:10.1029/92JC00127.

Fujii, Y., and M. Kamachi (2003), Three-dimensional analysis of temperature and salinity in the equatorial Pacific using a variational method with vertical coupled temperature-salinity empirical orthogonal function modes, *J. Geophys. Res.*, *108*(C9), 3297, doi:10.1029/2002JC001745.

Godfrey, J. S., and E. J. Lindstrom (1989), The heat budget of the equatorial western Pacific surface mixed layer, *J. Geophys. Res.*, *94*, 8007–8017, doi:10.1029/JC094iC06p08007.

Hasegawa, T., K. Ando, I. Ueki, K. Mizuno, and S. Hosoda (2013), Upper-ocean salinity variability in the tropical Pacific: Case study for quasidecadal shift during 2000s using TRITON buoys and ARGO floats, *J. Clim.*, *26*, 8126–8138. doi:10.1175/JCLI-D-12-00187.1.

Henocq, C., J. Boutin, G. Reverdin, F. Petitcolin, S. Arnault, and P. Lattes (2010), Vertical variability of near-surface salinity in the tropics: Consequences for L-band radiometer calibration and validation, *J. Atmos. Oceanic Technol.*, *27*, 192–209, doi:10.1175/2009JTECHO670.1.

Johnson, E. S., G. S. E. Lagerloef, J. T. Gunn, and F. Bonjean (2002), Surface salinity advection in the tropical oceans compared with atmospheric freshwater forcing: A trial balance, *J. Geophys. Res.*, *107*(C12), 8014, doi:10.1029/2001JC001122.

Juza, M., T. Penduff, J.-M. Brankart, and B. Barnier (2012), Estimating the distortion of mixed layer property distributions induced by the Argo sampling, *J. Oper. Oceanogr.*, *5*(1), 45–58.

Kalnay, E., et al. (1996), The NCEP/NCAR 40-year reanalysis project, *Bull. Am. Meteorol. Soc.*, *77*, 437–471.

Kessler, W. S. (1990), Observations of long Rossby waves in the northern tropical Pacific, *J. Geophys. Res.*, *95*, 5183–5217, doi:10.1029/JC095iC04p05183.

Kessler, W. S., L. M. Rothstein, and D. Chen (1998), The annual cycle of SST in the eastern Tropical Pacific, diagnosed in an ocean GCM, *J. Clim.*, *11*, 777–799.

Lagerloef, G., et al. (2008), The Aquarius/SAC-D Mission: Designed to meet the salinity remote-sensing challenge, *Oceanography*, *21*, 68–81.

Lagerloef, G., et al. (2013), Aquarius salinity validation analysis: Data version 2.0, *Aquarius Proj. Doc. AQ-014-PS-0016*, 36 pp. [Available at http://aquarius.nasa.gov/pdfs/AQ-014-PS-0016_AquariusSalinityDataValidation Analysis_DatasetVersion2.0.pdf.]

Lee, T., G. S. E. Lagerloef, M. M. Gierach, H. Kao, S. Yueh, and K. Dohan (2012), Aquarius reveals salinity structure of tropical instability waves, *Geophys. Res. Lett., 39*, L12610, doi:10.1029/2012GL052232.

Levitus, S. (1982), Climatological Atlas of the World Oceans, *NOAA Prof. Pap. 13*, 190 pp., U.S. Gov. Print. Off., Rockville, Md.

Lindstrom, E., R. Lukas, R. Fine, E. Firing, S.J. Godfrey, G. Meyers, and M. Tsuchiya (1987), The western equatorial Pacific Ocean circulation study. *Nature*, *330*, 533–537.

Lukas, R., and E. Lindstrom (1991), The mixed layer of the western equatorial Pacific Ocean, *J. Geophys. Res.*, *96*, 3343–3358, doi:10.1029/90JC01951.

Lukas, R., T. Yamagata, and J. P. McCreary (1996), Pacific low-latitude western boundary currents and the Indonesian throughflow, *J. Geophys. Res.*, *101*, 12,209–12,216, doi:10.1029/96JC01204.

Maes, C. (2000), Salinity variability in the equatorial Pacific Ocean during the 1993–98 period, *Geophys. Res. Lett.*, *27*, 1659–1662, doi:10.1029/1999GL011261.

Maes, C. (2008), On the ocean salinity stratification observed at the eastern edge of the equatorial Pacific warm pool, *J. Geophys. Res.*, *113*, C03027, doi:10.1029/2007JC004297.

Maes, C., and S. Belamari (2011), On the impact of salinity barrier layer on the Pacific Ocean mean state and ENSO, *Sci. Online Lett. Atmos.*, *7*, 97–100.

Maes, C., J. Picaut, and S. Belamari (2002), Salinity barrier layer and onset of El Niño in a Pacific coupled model, *Geophys. Res. Lett.*, *29*(24), 2206, doi:10.1029/2002GL016029.

Maes, C., J. Picaut, Y. Kuroda, and K. Ando (2004), Characteristics of the convergence zone at the eastern edge of the Pacific warm pool, *Geophys. Res. Lett.*, *31*, L11304, doi:10.1029/2004GL019867.

Maes, C., J. Picaut, and S. Belamari (2005), Importance of salinity barrier layer for the buildup of El Niño. *J. Clim.*, *18*, 104–118.

Maes, C., K. Ando, T. Delcroix, W. S. Kessler, M. J. McPhaden, and D. Roemmich (2006), Observed correlation of surface salinity, temperature and barrier layer at the eastern edge of the western Pacific warm pool, *Geophys. Res. Lett.*, *33*, L06601, doi:10.1029/2005GL024772.

McPhaden, M. J., and J. Picaut (1990), El Niño-Southern Oscillation displacement of the western equatorial Pacific warm pool, *Science*, *250*, 1385–1388.

McPhaden, M. J., F. Bahr, Y. Du Penhoat, E. Firing, S. P. Hayes, P. P. Niiler, P. L. Richardson, and J. M. Toole (1992), The response of the western equatorial Pacific ocean to westerly wind bursts during November 1989 to January 1990, *J. Geophys. Res.*, *97*, 14,289–14,302, doi:10.1029/92JC01197.

Palmer, T. N., and D. A. Mansfield (1984), Response of two atmospheric general circulation models to sea surface temperature anomalies in the tropical East and West Pacific, *Nature*, *310*, 483–485.

Picaut, J., F. Masia, and Y. du Penhoat (1997), An advective-reflective conceptual model for the oscillatory nature of the ENSO, *Science*, *277*, 663–666.

Picaut, J., M. Ioualalen, T. Delcroix, F. Masia, R. Murtugudde, and J. Vialard (2001), The oceanic zone of convergence on the eastern edge of the Pacific warm pool: A synthesis of results and implications for ENSO and biogeochemical phenomena, *J. Geophys. Res.*, *106*, 2363−2386, doi:10.1029/2000JC900141.

Qu, T., H. Mitsudera, and T. Yamagata (1999), A climatology of the circulation and water mass distribution near the Philippine coast, *J. Phys. Oceanogr.*, *29*, 1488–1505.

Qu, T., J. Gan, A. Ishida, Y. Kashino, and T. Tozuka (2008), Semiannual variation in the western tropical Pacific Ocean, *Geophys. Res. Lett.*, *35*, L16602, doi:10.1029/2008GL035058.

Qu, T., S. Gao, and R. Fine (2013), Subduction of South Pacific tropical water and its equatorward pathways as shown by a simulated passive tracer, *J. Phys. Oceanogr.*, *43*(8), 1551–1565, doi:10.1175/JPO-D-12-0180.1.

Reverdin, G., S. Morisset, D. Bourras, N. Martin, A. Lourenço, J. Boutin, C. Caudoux, J. Font, and J. Salvador (2013), Surpact: A SMOS surface wave rider for air-sea interaction, *Oceanography*, *26*(1), 4857, doi:10.5670/oceanog.2013.04.

Riser, S., L. Ren, and A. Wong (2008), Salinity in Argo: A modern view of a changing ocean, *Oceanography*, *21*, 56–67.

Rodier, M., G. Eldin, and R. Le Borgne (2000), The western boundary of the equatorial Pacific upwelling: Some consequences of climatic variability on hydrological and planktonic properties, *J. Oceanogr.*, *56*, 463–471.

Shinoda, T., and R. Lukas (1995), Lagrangian mixed layer modeling of the western equatorial Pacific, *J. Geophys. Res.*, *100*, 2523–2541, doi:10.1029/94JC02486.

Singh, A., T. Delcroix, and S. Cravatte (2011), Contrasting the flavors of El Niño-Southern Oscillation using sea surface salinity observations, *J. Geophys. Res.*, *116*, C06016, doi:10.1029/2010JC006862.

Song, Y. T., S. Yueh, J.-H. Moon, and T. Qu (2013), Assessing the seasonal variability of the global sea surface salinity, *J. Geophys. Res.*, in press.

Sprintall, J., and M. Tomczak (1992), Evidence of the barrier layer in the surface layer of the tropics, *J. Geophys. Res.*, *97*, 7305–7316, doi:10.1029/92JC00407.

Takahashi, K., A. Montecinos, K. Goubanova, and B. Dewitte (2011), ENSO regimes: Reinterpreting the canonical and Modoki El Niño, *Geophys. Res. Lett.*, *38*, L10704, doi:10.1029/2011GL047364.

Yu, J.-Y., and H.-Y. Kao (2007), Decadal changes of ENSO persistence barrier in SST and ocean heat content indices: 1958–2001, *J. Geophys. Res.*, *112*, D13106, doi:10.1029/2006JD007654.